Flowfield Investigation of a Supercruise Fighter Model

David E. Reubush,* E. Ann Bare,* and Steven F. Yaros*
NASA Langley Research Center, Hampton, Virginia
and
Jeffrey A. Yetter†
Boeing Military Airplane Company, Seattle, Washington

A cooperative NASA Langley-Boeing investigation was conducted in the Langley 16-ft Transonic Tunnel to survey the flowfield around a model of a supersonic cruise fighter configuration. In this investigation a model of a Boeing-designed supersonic cruise fighter configuration formerly utilized in afterbody-nozzle performance investigations was surveyed with a single multiholed probe to determine local values of angle of attack, side flow, and Mach number. The investigation was conducted at Mach numbers of 0.6, 0.9, and 1.2 at angles of attack from 0 to 10 deg. The purpose of the investigation was to provide a data base of experimental data for use in verification of theoretical methods, and to compare the experimental data with predictions from currently available theoretical techniques. The comparisons of experimental data with theoretical predictions show that the theoretical techniques give a qualitative estimate of the flowfield, but much work will be required to give good quantitative results.

Nomenclature

M = Mach number
MS = model station
α = angle of attack
β = sideflow angle

Introduction

THE next generation of high-performance aircraft will be required to operate over a wide range of flight conditions to meet the desired mission requirements. The designers of these aircraft will be faced with a multitude of design options, particularly regarding the aircraft propulsion system and how it is integrated with the airframe. These options will include such variables as engine location, inlet location, inlet type, nozzle location, nozzle type, etc. The effects of all of these variables on configuration performance must be evaluated and performance trades must be made to arrive at the optimum configuration to meet the mission requirements. It is recognized that the construction and testing of wind tunnel models to evaluate all of the configuration variables would be physically as well as financially impossible. As a result, most performance trade studies involving variations in aircraft configuration are made using theoretical techniques with only the most promising configurations being wind tunnel tested. In order to develop confidence in the theoretical techniques, sufficient comparisons between the theoretical predictions and good experimental data must be made.

As part of a NASA program to provide an experimental data base suitable for theory verification, the NASA Langley Research Center and the Boeing Military Airplane Company entered into a cooperative agreement to test, in Langley facilities, a Boeing designed and constructed wind tunnel model of an advanced supersonic cruise fighter. The wind tunnel model, which simulated a Mach 2.0 design, 49,000-lb aircraft was originally designed as a research model for advanced exhaust nozzle concepts.[1-5] The objective of the current investigation was to survey the model flowfield to provide local values of angle of attack, side flow, Mach number, etc., which could be utilized in the development and verification of theoretical techniques useful for trade studies. In addition, predictions from currently available theoretical techniques were compared with the experimental data to evaluate the current state of the art.

The wind tunnel investigation was conducted in the Langley 16-ft Transonic Tunnel at Mach numbers of 0.6, 0.9, and 1.2 at angles of attack of 0, 5, and 10 deg (7.5 deg maximum at $M=1.2$). Flowfield data were obtained by use of a single multiholed probe mounted on a survey apparatus.

Experimental Methods

Wind Tunnel and Tests

The investigation was conducted in the Langley 16-ft Transonic Tunnel. This facility is a continuous-flow, single-return, atmospheric wind tunnel with capability of continuously variable Mach numbers from 0.0 to 1.3. A detailed description of the tunnel can be found in Refs. 6 and 7.

This investigation was conducted at Mach numbers of 0.6, 0.9, and 1.2. Angle of attack was set at 0, 5, and 10 deg at the two subsonic Mach numbers and at 0, 5, and 7.5 deg at $M=1.2$. Reynolds number based on mean geometric chord varied from 3.1 to 3.9×10^6

Model and Support System

This investigation was conducted with a 10.5%-scale model of a twin-engine fighter aircraft designed as a supercruiser. Figure 1 shows a sketch of the supercruiser, while Fig. 2 is a photograph of the model installed in the Langley 16-ft Transonic Tunnel. All tests were conducted with 0.1-in.-wide boundary-layer transition strips of No. 100 silicon carbide. Transition strips were located 2.0 in. aft of the nose and 0.20 in. normal to the leading edge of the upper and lower surfaces of the wings. Although the fighter configuration included a canard for control purposes, this investigation was conducted with the canard removed. The model was supported in the tunnel by a sting-strut support in which the strut replaced the vertical tail. The strut had an NACA 0006 airfoil section with a 60-deg sweep, 29.17-in. chord, and a maximum thickness of 1.75 in.

Presented as Paper 84-1331 at the AIAA/SAE/ASME 20th Joint Propulsion Conference, Cincinnati, Ohio, June 11-13, 1984; received July 9, 1984; revision received Oct. 19, 1984.

*Research Engineer, Propulsion Aerodynamics Branch, Transonic Aerodynamics Division. Member AIAA.
†Senior Engineer. Member AIAA.

The configuration had a delta wing with 68-deg leading-edge sweep and an aspect ratio of 1.5. The model had a wing span of 37.8 in. and an overall length of 100.5 in. The configuration was designed for a cruise speed of Mach 2 with a design lift coefficient of 0.10. The trim condition for the vehicle was established from the criterion that the vehicle be 5% unstable subsonically, which resulted in the vehicle being 4% stable for the supersonic design case.

Flowfield Survey Probe and Translating Mechanism

A three pressure prism probe was used for the flowfield measurements. The probe was constructed of three 0.020-in. i.d. stainless steel tubes. The tips of the two outer tubes were cut at an angle of 45 deg with respect to the probe centerline. The local flow angle is proportional to the difference in pressure measured by the outer two orifices normalized by the difference in pressure between the center orifice and the average of the outer two. The local Mach number is proportional to the average of the outer pressures normalized by the center pressure. The variation of these two parameters with Mach number and flow angle was determined by an in-tunnel calibration. Calibration tests were made at Mach numbers from 0.4 to 1.28 at angles of attack from -15 to $+15$ deg. The measured pressures obtained during the experimental investigation were reduced to local Mach number and flow angle by use of a double interpolation scheme.

The survey probe was moved through the flowfield by a translating mechanism mounted on the tunnel angle-of-attack strut. The probe was attached to the mechanism by a support sting 1.00 in. in diameter. The translating mechanism allowed the survey probe to be positioned within a cylindrical volume approximately 4 ft long and 4 ft in diameter. The probe may be translated in both the longitudinal and lateral directions and rolled about the axis of the probe support sting. The actual longitudinal location of the survey region is determined by the length of the probe support sting.

Procedure

Flowfield measurements were obtained in three survey areas. Areas 1 and 2 were below and above the wing, respectively, at model station 70.50 (see Fig. 1). Area 3 was forward and above the wing at model station 50.50 (see Fig.1). Surveys were made for each area in separate tunnel runs. The survey probe was positioned at the desired model station before tunnel startup. Flowfield surveys were then performed by systematically varying the support blade roll angle and survey sting radial position. The data were initially taken with the survey probe in an upright configuration. The probe was then rolled 90 deg and the run repeated. The results from the two runs were interpolated to obtain local values of angle of attack, side flow, and Mach number. It is estimated that the angles of attack and sideflow angles are within ± 0.05 deg and the Mach numbers are within ± 0.005.

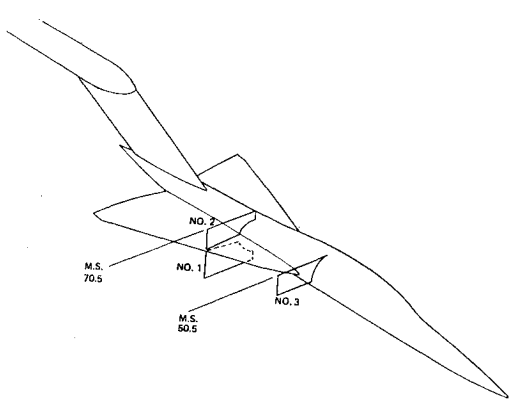

Fig. 1 Supercruise fighter showing survey areas.

Presentation and Discussion of Experimental Results

Because there is a large quantity of data that indicates there are only small Mach number effects on the various measured quantities, only the data obtained at $M=0.9$ will be presented. Also, since the character of the flow is similar at lifting conditions, only data at 0 and 5 deg will be presented. (A complete set of data may be found in Ref. 8.) Results of this investigation are presented as contours of local angle of attack, sideflow angle, and Mach number, as well as a composite vec-

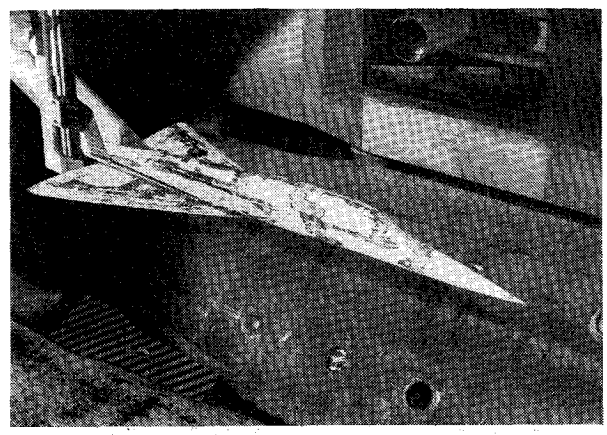

Fig. 2 Flowfield survey probe and model installed in Langley 16-ft Transonic Tunnel.

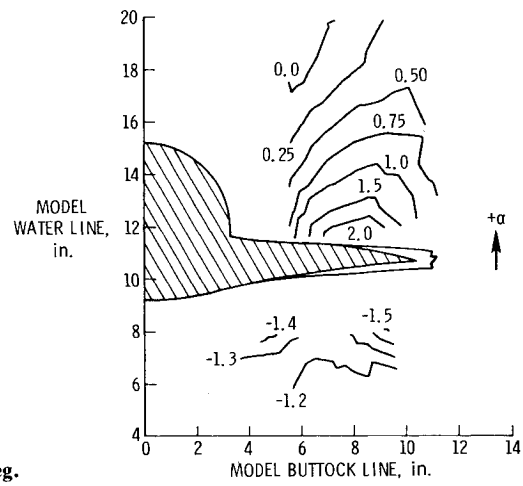

a) $\alpha=0$ deg.

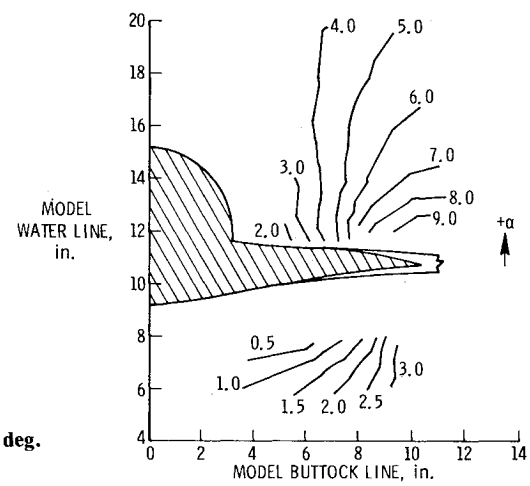

b) $\alpha=5$ deg.

Fig. 3 Local angle-of-attack contours for areas 1 and 2 (MS = 70.50 in.); $M=0.90$.

tor plot visualizing the direction of local flow (in a plane perpendicular to the model longitudinal axis). In the composite vector plots the magnitude of each vector represents the resultant of the local angle of attack and side flow. (Note: The scale factor may differ among different survey areas and test conditions.)

Figure 3 presents contours of local angle of attack for survey areas 1 and 2 at angles of attack of 0 and 5 deg. For survey area 1, below the wing, the measured angles of attack are always less than the freestream value. For 0-deg freestream angle of attack the contours of constant local angle of attack are relatively parallel to the wing and become increasingly lower than freestream as the lower surface of the wing is approached. This indicates that the incoming flow is forced to bend downward to flow around the wing. At lifting conditions (angles of attack of 5 and 10 deg) the contours shift such that the lowest angles of attack are inboard and the angle increases spanwise. For survey area 2, above the wing, the measured angles of attack vary from less than freestream to considerably above freestream. At 0-deg angle of attack the local angle of attack varies from 2.0 deg close to the surface of the wing to 0 deg above the wing and toward the fuselage. At lifting conditions ($\alpha > 0$ deg) the contours of local angle of attack increase from values less than freestream close to the fuselage to values twice freestream near the wing outboard edge.

Figure 4 presents contours of constant local side flow for survey areas 1 and 2. For survey area 1 the local side flows are generally directed spanwise away from the body and increase as the wing leading edge is approached. An increase in angle of attack results in an increase in local side flow as well as an increase in the magnitude of the side-flow gradient across the measurement region. For survey area 2 the local side-flow characteristics vary considerably with angle of attack. The magnitude of the side flows and the side-flow gradients across the measurement area increase with angle of attack. Also, typically the magnitude of the local side flow decreases in the direction away from the wing.

Figure 5 presents the contours of constant local Mach number in survey regions 1 and 2. These contours may be considered representative of the chordwise flow characteristics. For survey area 1 at positive lift conditions ($\alpha > 0$ deg) the local Mach numbers are less than freestream, as would be expected for a region of positive pressure coefficient. Also at lifting conditions the Mach number appears to increase as either the body or wing is approached; however, the Mach number gradient across the survey region is generally small. For the 0-deg angle-of-attack case the local Mach numbers are above freestream, as would be expected for a condition of no lift and low pressure. For survey region 2, above the wing, the maximum local Mach number is obtained inboard and toward the wing surface. Typically, the Mach gradient across the survey region increased with angle of attack. At subsonic conditions an increase in angle of attack produced the expected increase in local Mach numbers.

A summary of the local flowfield characteristics for survey areas 1 and 2 is shown in Fig. 6 as a composite vector plot visualizing the direction of local flow in the survey plane perpendicular to the model longitudianal axis. For survey area 1 at 0-deg angle of attack the flow is directed downward away from the wing, while at lifting conditions the flow is directed in a spanwise direction with a slight upward component near the leading edge. This upward component near the leading

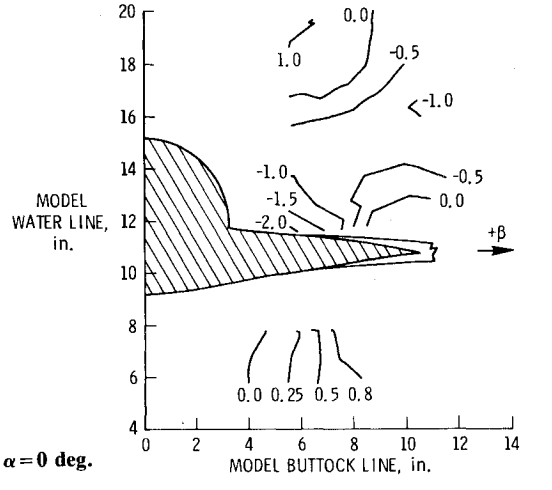

a) $\alpha = 0$ deg.

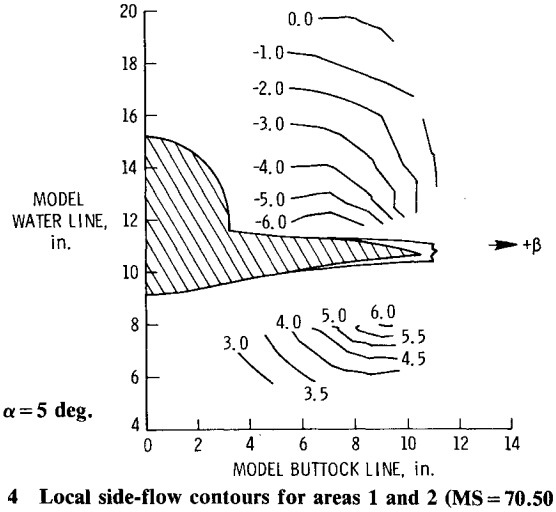

b) $\alpha = 5$ deg.

Fig. 4 Local side-flow contours for areas 1 and 2 (MS = 70.50 in.); $M = 0.90$.

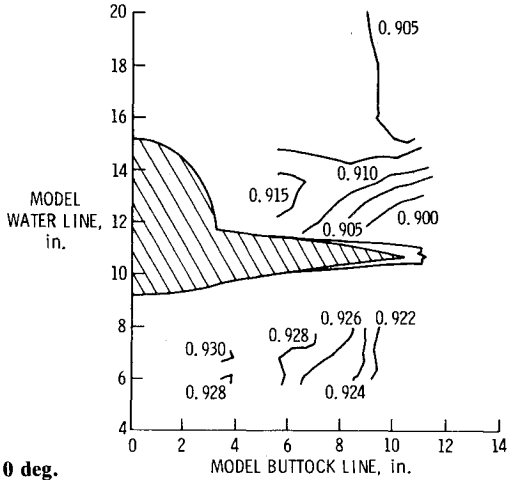

a) $\alpha = 0$ deg.

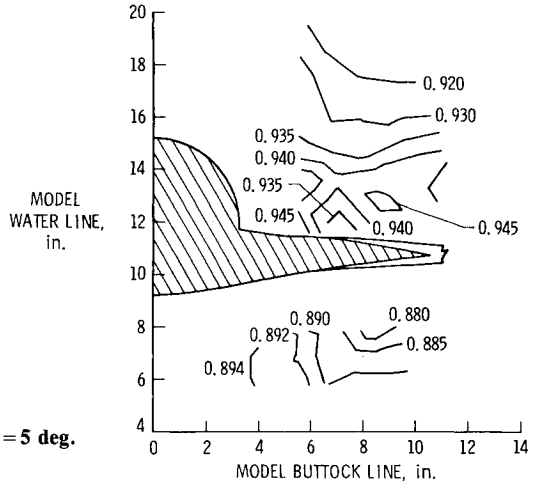

b) $\alpha = 5$ deg.

Fig. 5 Local Mach number contours for areas 1 and 2 (MS = 70.50 in.); $M = 0.90$.

edge is indicative of the flow from below the wing moving around the leading edge into the vortex which forms above the upper surface near the leading edge. For survey area 2, above the wing, the tendency toward a rotational flow can be seen even at 0-deg angle of attack. The flow tends to rise upward away from the wing and bend toward the fuselage.

Data obtained in survey area 3 which is forward of the wing are presented in Figs. 7-10. Here the dominant flow phenomena are due to the flow passing around the body. Figure 7 presents the contours of constant local angle of attack for survey area 3. As would be expected, the local angle of attack is above model angle of attack near the body and decreases away from the body.

Figure 8 presents the contours of constant local side flow for area 3. Again, as would be expected from visualizing the flow being forced to pass around the body at 0-deg angle of attack the side flow (which is directed outboard) is greatest near the body and decreases in an outboard direction. At angle of attack, the side-flow contours indicate that the flow is directed toward the body very near the body. Slightly away from the body the flow then changes direction to outboard. This flow toward the body is probably due to the flow trying to fill in the low-pressure region created near the body.

Local Mach number contours for survey area 3 are shown in Fig. 9. At an angle of attack of 0 deg the local Mach numbers are very near freestream. Increasing the angle of attack to 5 deg results in increased local Mach numbers which are greatest near the body. At angles of attack above 5 deg the local Mach numbers increase even further.

Figure 10 summarizes the flowfield at survey area 3 with the composite vector plots. At 0-deg angle of attack the flow is primarily directed outboard away from the body and upward with the magnitude of the vector decreasing away from the body. At angle of attack the flow is primarily directed upward with a slight inboard component near the body and a slight outboard component away from the body.

Numerical Flow Prediction

A number of theoretical methods were used to predict the flowfields around the model. Certain criteria were used to assess the applicability of each of the theoretical methods. Solution accuracy, integrity of the geometric model, operational ease, and computational time were the most important criteria. In the final analysis, for supersonic cases, a three-dimensional Euler equation marching code, STEIN, was chosen over a surface paneling code, the PAN AIR pilot code. Although the latter program was applicable to a wide range of geometric configurations and has reached a high level of technical development,[9] recent studies[10] have shown that it is less accurate relative to the STEIN code and substantially more expensive to operate.

A similar situation developed in the search for a transonic code. Ultimately, a small-disturbance code, WIBCO, was chosen over a full-potential code, FLO-30, which is the latest member of a family of FLO-codes,[11-13] each of which is capable of handling a more complex wing-body configuration. Investigation of some FLO-30 calculations,[14] however, indicated that the method by itself was capable of solutions for fuselages of only moderate complexity, particularly if the wing was of low aspect ratio. Since many of the fighter cross sections varied considerably from an axisymmetric shape, it was decided that WIBCO would be the better choice, in spite of the small-disturbance approximation applied in the calculations.

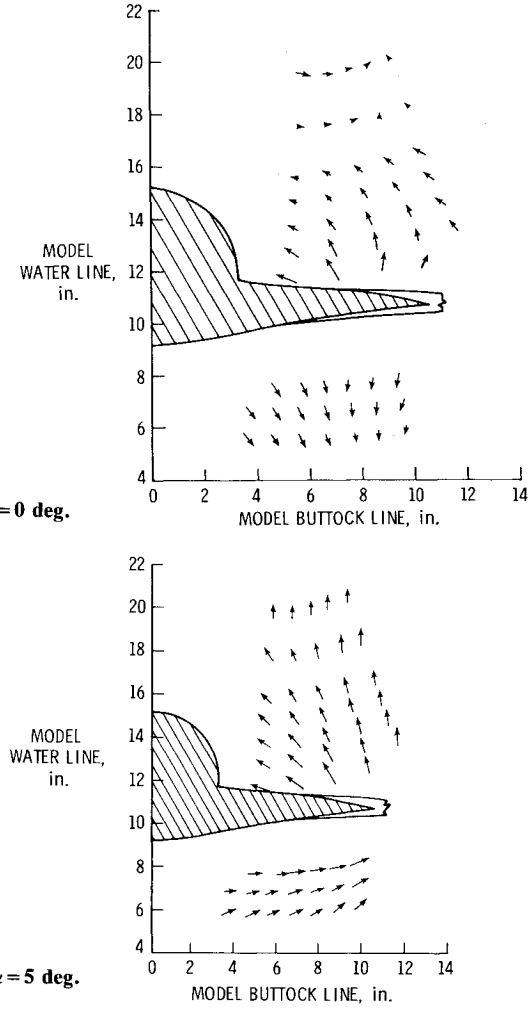

Fig. 6 Local flowfield for areas 1 and 2 (MS=70.50 in.); $M=0.90$.

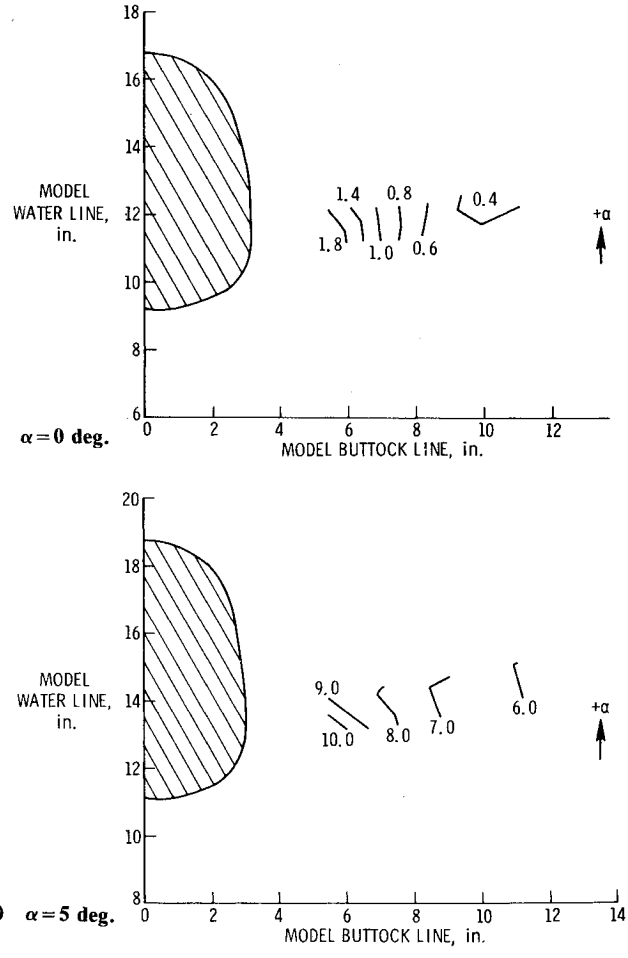

Fig. 7 Local angle-of-attack contours for area 3 (MS=50.50 in.); $M=0.90$.

The results presented herein are solely from the transonic code, WIBCO. STEIN, the supersonic code,[15,16] while providing satisfactory results for flows in which there were no imbedded subsonic regions, was unable to successfully negotiate its marching solutions past areas of complex geometry, such as the wing/fuselage juncture, below $M = 1.9$. This was not unexpected since neither WIBCO nor STEIN had been developed for application to such complex configurations as fighters.

The WIBCO transonic code was developed by Boppe[17] primarily to apply the solution of the small-disturbance potential equation to arbitrary wing and body geometries. Recognizing the increasing complexity of traditional grid transformations as configurations become more three-dimensional, Boppe avoided these problems by imbedding fine Cartesian grids into an overall coarse grid in regions where more flow detail is required. The wing and body fine-grid systems are constructed to totally encapsulate their portions of the geometry and provide computations over a much smaller area of the flow. These two fine-grid systems overlap and transfer information to each other, as well as to the crude-grid system, during the course of the iterations. It should be noted that although the body fine-grid system is a regular Cartesian grid, the wing fine-grid system is swept and tapered according to the planform shape. The finite difference approximations are straightforward. Central differencing is used throughout except in areas of local supersonic flow, in which upwind differencing is used for most of the second derivative terms. In keeping with the near-isentropic nature of the flow, nonconservative difference operators are used, although it is acknowledged that results will become less accurate with increasing shock strength. For a wing-body configuration, the solution begins with an arbitrary number (typically 100) of successive line-overrelaxation sweeps of the crude grid to provide a starting solution for the fine-grid systems. The second phase of the solution involves a sweep of the wing fine-grid, the body fine-grid, and the crude-grid systems with appropriate updating of overlapping areas. Approximately 80 second-phase iterations are usually required. Since none of the grid systems are body or wing fitted, boundary conditions are applied at mesh points nearest the actual surfaces. Corrections are applied at these points for wing-surface slope and body displacement as well as for local flow inclination.

The version of WIBCO used herein is the basic wing-body code. Further capabilities have been added,[18] including the fine-grid system applied to pylons, nacelles, and winglets, as well as a scheme for modeling inlet spillage and exhaust interference effects. Previous results for other fighter-type configurations have been presented in Refs. 19 and 20.

The WIBCO code was capable of generating solutions for all nine points in the Mach number/angle-of-attack test matrix. Typical results are shown as Figs. 11-13, which are at a freestream Mach number of 0.9 and angle of attack of 5 deg. It can be seen that both the local angle of attack and sideslip exhibit more activity than the predictions indicate. This effect increases strongly with increasing Mach number and is especially noticeable in the greatly increased inflow over the wing. Local Mach number predictions at the lowest two freestream Mach numbers are reasonable, but at the highest Mach number become chaotic, both above and below the wing.

At the highest angles of attack a vortex is shed from the leading edge of the wing. It is not surprising that the WIBCO

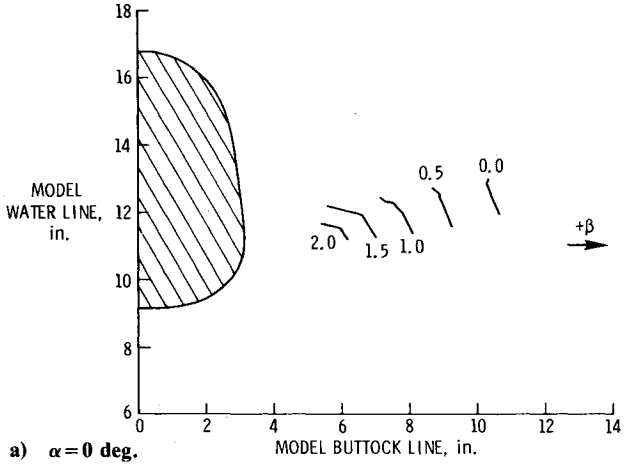

a) $\alpha = 0$ deg.

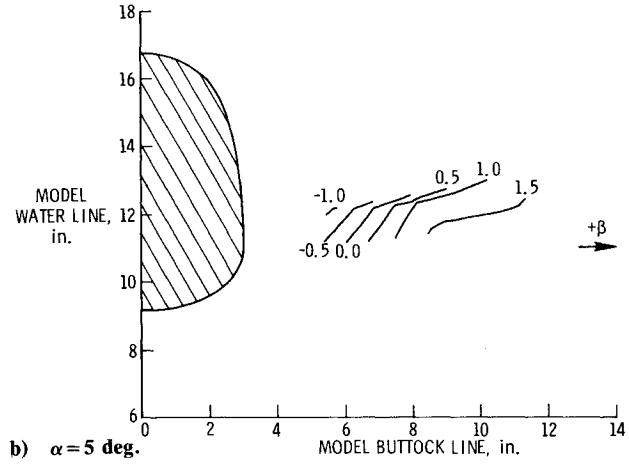

b) $\alpha = 5$ deg.

Fig. 8 Local side-flow contours for area 3 (MS = 50.50 in.); $M = 0.90$.

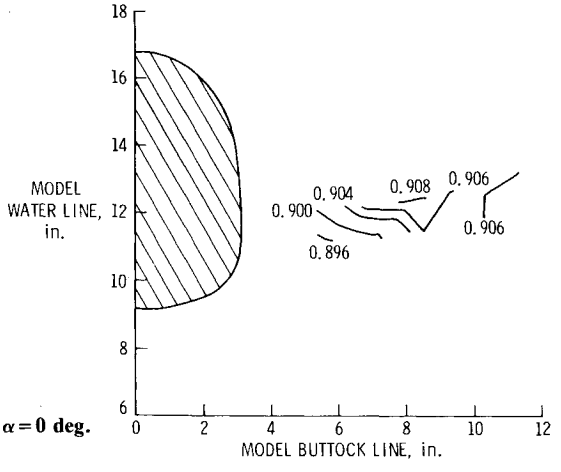

a) $\alpha = 0$ deg.

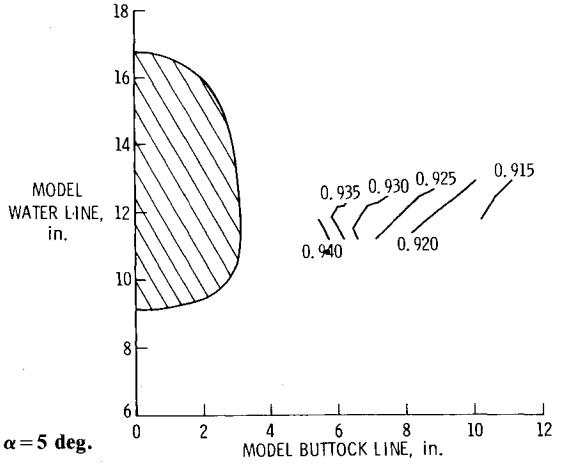

b) $\alpha = 5$ deg.

Fig. 9 Local Mach number contours for area 3 (MS = 50.50 in.); $M = 0.90$.

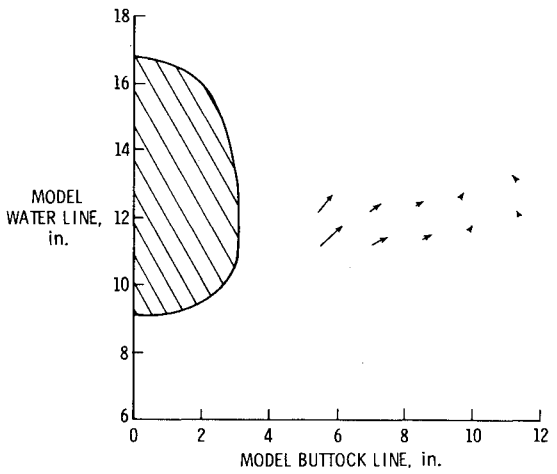

a) $\alpha = 0$ deg.

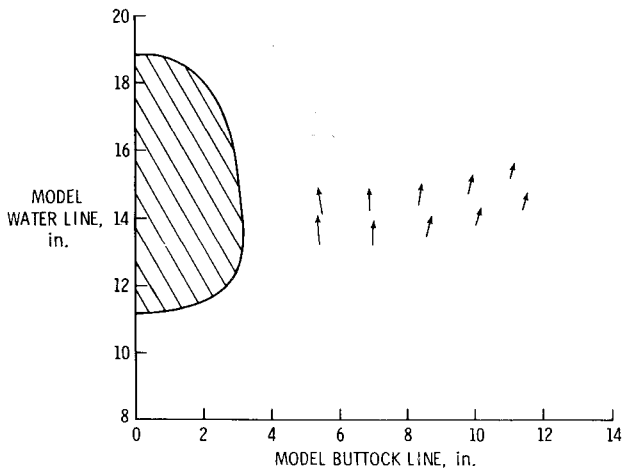

b) $\alpha = 5$ deg.

Fig. 10 Local flowfield for area 3 (MS = 50.50 in.); $M = 0.90$.

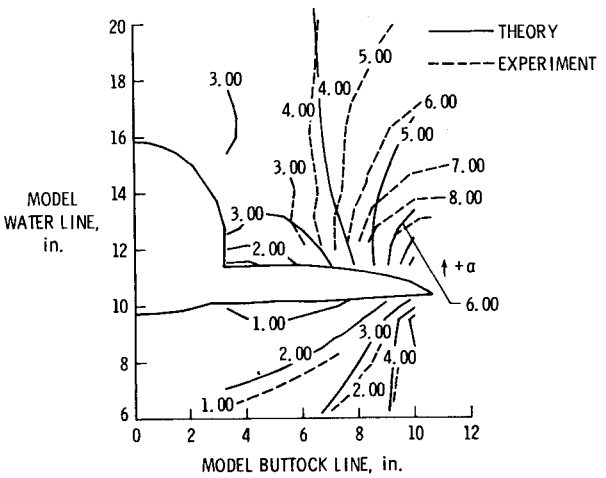

Fig. 11 Comparison of measured and predicted local angle-of-attack contours at $M = 0.90$, $\alpha = 5$ deg.

code is unable to predict this flow development, for codes capable of doing such are rather specialized. However, even though WIBCO is partially unsuccessful in these cases, it is pointed out that the predictions below the wing where the flow is much better behaved are reasonable in most cases.

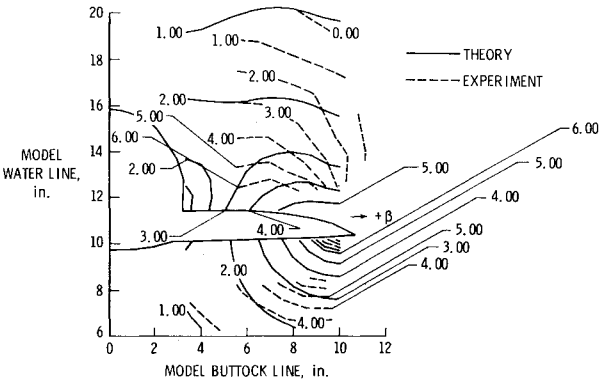

Fig. 12 Comparison of measured and predicted local side-flow contours at $M = 0.90$, $\alpha = 5$ deg.

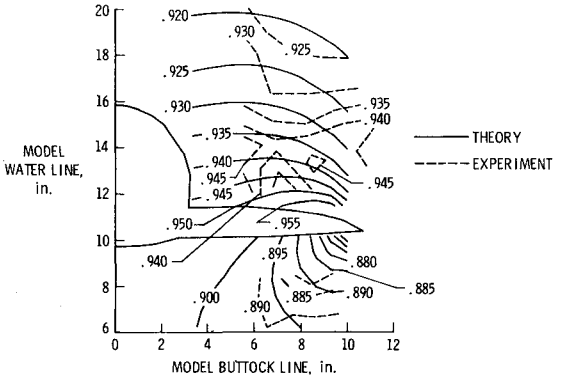

Fig. 13 Comparison of measured and predicted local Mach number contours at $M = 0.90$, $\alpha = 5$ deg.

Concluding Remarks

The flowfield investigation of a supersonic cruise fighter configuration has yielded a substantial data base of flowfield characteristics such as local angle of attack, local side flow, and local Mach number which can be utilized in the development of advanced computational techniques. As would be expected for this type of configuration, the experimental data have indicated that the flow under the wing is the most benign, being shielded by the wing, while the flow above the wing is most complex, being dominated by the leading-edge vortex. The comparison of the experimental data with predictions of currently available theoretical techniques indicates that while the analytical methods are capable of giving a qualitative estimate of the flowfield, much work will be required to give good quantitative results.

References

[1]Hutchinson, R.A., Petit, J.E., Capone, F.J., and Whittaker, R.W., "Investigation of Advanced Thrust-Vectoring Exhaust Systems for High Speed Propulsive Lift," AIAA Paper 80-1159, July 1980.

[2]Capone, F.J., Reubush, D.E., Petit, J.E., and Hutchinson, R.A., "Nacelle/Nozzle Integration for Supersonic Fighter Aircraft," NASA CP-2162, 1981, pp. 655-694.

[3]Paulson, J.W. Jr., "Thrust-Induced Aerodynamics of STOL Fighter Configurations," NASA CP-2162, 1981, pp. 695-712.

[4]Capone, F.J. and Reubush, D.E., "Effect of Thrust Vectoring and Wing Maneuver Devices on Transonic Aeropropulsive Characteristics of a Supersonic Fighter Aircraft," NASA TP-2119, 1983.

[5]Capone, F.J. and Reubush, D.E., "Effect of Varying Podded Nacelle/Nozzle Installations on Transonic Aeropropulsive Characteristics of a Supersonic Fighter Aircraft," NASA TP-2120, 1983.

[6]Peddrew, K.H., "A User's Guide to the Langley 16-Foot Transonic Tunnel," NASA TM-83186, 1981.

[7]Corson, B.W. Jr., Runckel, J.F., and Igoe, W.B., "Calibration of the Langley 16-Foot Transonic Tunnel with Test Section Air Removal," NASA TR R-423, 1974.

[8]Yetter, J.A., Salemann, V., and Sussman, M.B., "Inlet Flowfield Investigation: Part I—Transonic Flowfield Survey," NASA CR-172239, 1983.

[9]Ehlers, F.E., Epton, M.A., Johnson, F.T., Magnus, A.E., and Rubbert, P.E., "An Improved Higher Order Panel Method for Linearized Supersonic Flow," AIAA Paper 78-15, 1978.

[10]Landrum, E.J. and Miller, D.S., "Assessment of Analytic Methods for the Prediction of Aerodynamic Characteristics of Arbitrary Bodies at Supersonic Speeds," AIAA Paper 80-0071, 1980.

[11]Caughey, D.A. and Jameson, A., "Numerical Calculation of Transonic Potential Flow About Wing-Body Combinations," AIAA Paper 77-677, 1977.

[12]Caughey, D.A., Newman, P.A., and Jameson, A., "Recent Experiences With Three-Dimensional Transonic Potential Flow Calculations," NASA TM-78733, 1978.

[13]Caughey, D.A. and Jameson, A., "Recent Progress in Finite-Volume Calculations for Wing-Fuselage Combinations," AIAA Paper 79-1513, 1979.

[14]Verhoff, A. and O'Neil, P.J., "Extension of FLO Codes to Transonic Flow Prediction for Fighter Configurations," *Transonic Aerodynamics*, edited by David Nixon, AIAA, New York, 1982, pp. 467-487.

[15]Marconi, F., Salas, M., and Yaeger, L., "Development of a Computer Code for Calculating the Steady Super/Hypersonic Inviscid Flow Around Real Configurations, Vol. I—Computational Technique," NASA CR-2675, 1976.

[16]Marconi, F. and Yaeger, L., "Development of a Computer Code for Calculating the Steady Super/Hypersonic Inviscid Flow Around Real Configurations," Vol. II—Code Description," NASA CR-2676, 1976.

[17]Boppe, C.W., "Transonic Flow Field Analysis for Wing-Fuselage Configurations," NASA CR-3243, 1980.

[18]Boppe, C.W. and Stern, M.A., "Simulated Transonic Flows for Aircraft With Nacelles, Pylons, and Winglets," AIAA Paper 80-0130, 1980.

[19]Yaros, S.F., "Evaluation of Two Analytical Methods for the Prediction of Inlet Flow Fields in the Vicinity of Generalized Forebodies," AIAA Paper 82-0959, 1982.

[20]Yaros, S.F., "Theoretical and Experimental Engine-Inlet Flow Fields for Fighter Forebodies," NASA TP-2270, 1984.